RESEARCH ARTICLE



On the interaction between Kelvin waves at different phase speeds and the background flow

Ahmed A. Shaaban | Paul E. Roundy

Department of Atmospheric and Environmental Sciences, University at Albany, State University of New York, Albany, New York USA

Correspondence

A. A. Shaaban, Department of Atmospheric and Environmental Sciences, University at Albany, State University of New York, Albany, NY, USA. Email: alasheen@albany.edu

Funding information

National Science Foundation, Grant/Award Number: 1560627

Abstract

Kelvin waves have been theorized to be absorbed near the critical layer, where the phase speed matches the speed of the background flow. Nevertheless, it is not clear through observations how the structure of the Kelvin waves evolves near the critical layer or in response to vertical wind shear with or without a critical layer. A novel varying-coefficient regression technique that has been used to study evolving relationships across the seasonal cycle is used to capture how the wavelet-filtered waves with a specific phase speed appear in different background winds or vertical shear regimes or a combination of both. Results show a relaxation of the in-phase relationship between the zonal wind and geopotential height anomalies at slower Doppler-shifted speeds, followed by the appearance of the Gill pattern at further reduction of the Doppler-shifted speed, demonstrating a lack of dominant Kelvin wave signals in those conditions. We define the "observed critical layer" as the layer where the signals consistent with Kelvin waves fade away irrespective of the value of the Doppler-shifted speed, which reduces to zero at the "theoretical critical layer." Results show that wave structures consistent with Kelvin waves are not present at the top of layer with westerly vertical shear of the zonal wind, yet they exist during the easterly vertical shear of the zonal wind. The second part of the paper presents the dispersion equation of the Kelvin wave under vertical wind shear. The phase speed of the Kelvin wave proportionally increases with the Richardson number (and hence proportionally decreases with the vertical wind shear). The Richardson number varies with the vertical resolution of the data used, adding uncertainty to the calculated phase speed of the wave in the presence of vertical wind shear.

KEYWORDS

background wind, critical layer, Kelvin wave, Richardson number, wind shear

1 INTRODUCTION

Internal gravity waves (David and Alexander, 2003) are absorbed by the flow before approaching the critical layer, at which the phase speed of the wave, with respect to an observer on the Earth, matches the speed of the flow moving in the same direction (Bretherton, 1966; John and Francis, 1967). Near the critical layer, the wavefront aligns with the flow, trapping the wave's momentum. Accordingly, the frequency of the wave relative to the flow diminishes to zero. The frequency of the wave relative to the flow is known as the Doppler-shifted frequency or

SHAABAN AND ROUNDY structure of the waves could be wiped when considering the bulk characteristics of the waves. Stratospheric Kelvin waves originate from vertically propagating atmospheric

quasi-Doppler-shifted frequency, as suggested by Gerkema et al. (2013). They used the prefix "quasi-" in order to distinguish the classical Doppler shifting that happened to occur between wave source and observer from that associated with two different observing references (i.e., those of the Earth and the flow), as is the case here.

Kelvin waves behave similarly to small-scale gravity waves as they approach critical layers (Holton, 1970; Richard, 1970). The absorption of Kelvin waves and small-scale gravity waves in the eastward flow and the absorption of Rossby-gravity waves and especially the small-scale gravity waves (Hamid et al., 2021b) in the westward flow contribute to the downward propagation of the zonal wind of the quasi-biennial oscillation (QBO; Baldwin et al., 2001), as suggested by Lindzen and Holton (Richard and James, 1968; James and Lindzen, 1972). The absorption of the Kelvin and small-scale gravity waves contributes to the descending of the stratospheric westerlies eventually forming the the westerly phase of the QBO, whereas the fading of small-scale gravity waves and to a lesser extent the Rossby-gravity waves are found to be associated with descending of the stratospheric easterly flow, which is associated with the formation of the easterly phase of the QBO (e.g., Ern and Preusse, 2009a,b; Yang et al., 2011, 2012; Kim and Chun, 2015a,b; Hamid et al., 2021a,b), indicating that the source of the downward-propagating zonal wind is the absorption of the upward waves' momentum, as theorized by Richard and James (1968).

Kelvin waves are not only absorbed by the mean flow via the critical layer interaction. Kelvin waves can transfer their momentum to the mean flow via radiative (Newtonian) cooling or mechanical (Rayleigh) damping, or both. In this paper, we focus only on the absorption of the Kelvin waves via the critical-layer interaction. Most studies on the interaction between Kelvin waves and the QBO either estimate the Kelvin, Rossby, and small-scale gravity waves' forcing of the QBO phases during specific events (e.g., Ern and Preusse, 2009a; Kim and Chun, 2015b) or find the activity of the waves, filtered at a bulk of wave numbers and frequencies, at a specific phase or event of the QBO (e.g., Yang et al., 2011; Das and Pan, 2013).

In this study, we analyze the structure of eastwardmoving waves, at specific phase speeds centered at a given geographical location and pressure level, as they vary with the speed or vertical shear of the background flow rather than with respect to the QBO phases or events. To do that, we apply a combination of wavelet filtering and a new form of linear regression. The wavelet filtering technique is used to construct indices associated with waves at specific phase speed and wavelength that might be more informative than tracing waves filtered at bulk of wave numbers and speeds (frequencies) in which details about the evolving

disturbances. The directly forced motions can be associated with different types of waves or forced disturbances in the stratosphere. Whether a given forced disturbance yields a Kelvin wave depends at a minimum on whether the quasi-Doppler-shifted dispersion curve includes a Kelvin wave at the time-scale of the forcing. When the direct forced signals at a given speed project directly onto Kelvin waves, Kelvin-like signals then appear in the regression maps on the same time-scales. The approach diagnoses Kelvin-wave-like signals when such waves dominate in a given background wind setting and reveals other types of disturbances under conditions that do not favor Kelvin waves, allowing us to intuit from the wave statistics whether Kelvin-wave signals are consistent with the theory. Non-Kelvin disturbances are anticipated under conditions in which Kelvin waves do not form, because forcing from the troposphere occurs over a wide range of scales, including those in which Kelvin waves cannot occur in the given environment (Murry and Garcia, 1987).

The characteristics of the Kelvin waves at phase speeds that are greater than, less than, or equal to the background flow speeds are documented using the 30 years of ERA-Interim reanalysis. To accomplish the objective, we use a novel regression method that enables us to set a specific value of a background state variable (such as background zonal wind at a given height) in order to diagnose the linear relationship between a wavelet-filtered predictor index and fields of data during the specified background condition. The wavelet and the regression techniques are discussed in Section 3. The behavior of the filtered waves at different background wind speeds is discussed in Section 4.1, followed by a discussion of the behavior of the wave during variable wind shears and background winds in Section 4.2. A dispersion equation for the Kelvin waves within background wind shear is derived in Section 5.

DATA 2

Daily ERA-Interim reanalysis data from 1979 to 2017 on a 2.5° grid were used (Dee et al., 2011). The data are gridded on pressure levels from 500 to 10 hPa. The vertical levels and the associated heights are shown in Figure 5, where the vertical grid size increases from nearly 1 km below 100 hPa to a few kilometers above 100 hPa. High-resolution radiosonde observations during the dynamics of the Madden Julian Oscillation (DYNAMO) field campaign were used to calculate the Richardson number (Johnson et al., 2019). Anomalies were constructed by first regressing the raw data against

391 **■** RMetS

1477870x, 2023, 751, Dawhoaded from https://mets.onlinelibrary.wiley.com/doi/10.1002/qi.4412 by Suny University At Albany, Wiley Online Library on [1705/2023]. See the Terms and Conditions (https://onlinelibrary.wiley.com/terms-and-conditions) on Wiley Online Library for rules of use; OA articles are governed by the applicable Creative Commons Licensea

the first four harmonics of the seasonal cycle and then subtracting the mean and predicted seasonal cycle of 1980-2010 from the raw data (Narapusetty et al., 2009). Data used to represent the background state conditions are based on the equatorial zonal mean of the zonal wind or wind shear.

3 **METHODS**

Wavelet-based indices 3.1

Contrary to the common technique of filtering Kevin waves between two distinct equivalent depths, frequencies, and wave numbers using the Fourier transform (Wheeler and Kiladis, 1999; Wheeler et al., 2000), data are filtered at a specific phase speed and wave number using wavelet filtering to study the interaction of the wave signal at a particular phase speed with a predetermined speed or vertical shear of the background flow, as we discuss in Section 3.2. The wavelet kernel is designed following Paul (2017b) and Ahmed and Roundy (2021) as a two-dimensional array – see Equation (1) – where the rows and the columns represent the time *t* and longitude *x*:

$$\psi(x,t) = \frac{1}{\sqrt{a\pi}} \frac{1}{\sqrt{b\pi}} \cos[2\pi (f_x x - f_t t)]$$

$$\times \exp\left(-\frac{x^2}{b}\right) \exp\left(-\frac{t^2}{a}\right) \tag{1}$$

The length of the time dimension is 200 days, which enables us to capture slow waves. The longitudinal dimension matches the reanalysis data resolution 2.5° with 144 points in the 360°. Although wave number 4 is targeted, because it is a center of strong Kelvin wave activity, previous studies (e.g., Wheeler and Kiladis, 1999), the localized filter implies a superposition between plane waves of different wave numbers that peak at the targeted wave number (wave number 4), a price paid for the sake of the localization. Parameters a and b are usually called the scaling factors, f_x and f_t are the spatial and temporal frequencies. Parameter a is related to the temporal frequencies f_t as $a = 8(2\pi f_t/2\pi)^{-3/2}$ in order to localize each scale to include a similar number of cycles in the template. b was set to 8,000 using trial-and-error method. To apply the filter, the kernel is centered at the base longitude at 80° E along the Equator, as we are interested in Kelvin waves over the Indian Ocean, and at a particular day of the reanalysis, so the dot product between the kernel and the corresponding block of reanalysis data is the value of the wave index at that day. We used the zonal wind anomalies at different pressure levels to create the wavelet base indices at different levels. To find the value for the next day, the kernel is slid 1 day ahead and the same dot product is repeated. Signals that are selected here represent a tiny part of the spectrum demonstrated by Wheeler and Kiladis (1999) that contains Kelvin-wave-like signals (e.g., Paul, 2020), though they may also include non-Kelvin components.

The wavelet index is the signal in the reanalysis data centered at the base longitude that best projects onto the two-dimensional wavelet kernel. This index serves as the independent variable of the regression analysis. As reanalvsis data are reported relative to an observer on the Earth, then the phase speed c of the patterns correlated with this wavelet index is the speed relative to an observer on the Earth, which could be calculated as f_t/f_x . We refer to the wavelet indexes with their phase speeds. For example, the 20 m·s⁻¹ index refers to the dot product of the 20 m·s⁻¹ wavelet kernel with the reanalysis. Hence, the 20 m·s⁻¹ index used in regression model targets patterns correlated with the 20 m·s⁻¹ signal at the base point and the pressure level

The varying-coefficients wavelet regression and statistical significance test

The horizontal or vertical structure of the waves characterized by specific phase speeds is found by regressing dynamical fields like zonal wind anomalies (predictand), against a specific phase-speed wavelet index (predictor). This type of regression is called wavelet regression because the wavelet technique is used to construct the predictor. This simple linear regression does not enable us to study the structure of waves at a specific background condition (speed, wind shear, static stability) as simple linear regression has no information on the background conditions associated with the active periods of the wave.

Paul (2017a) developed a new form of linear regression that allows regression coefficients to evolve continuously across the calendar. The variance of the predictor was regressed against the seasonal cycle, and the same also for the covariance between the predictor and predictand. The ratio of the modeled variance and covariance on a specific day yields the regression slope coefficients on that day of the year. The variance of the predictor and covariance between predictor and predictand have seasonal cycles, so that a fit of the seasonal cycle can be used to create seasonally varying regression slope coefficients continuously. Yet these variance and covariance quantities can vary with other factors beyond the seasonal cycle, like the mean state background zonal wind. In this study, instead of allowing regression slopes to vary with the seasonal cycle, we allow them to vary with the background zonal wind, background vertical shear of the zonal wind, and a combination of both. We replace the harmonics of the seasonal cycle in the matrix X of Paul (2017a) with time series of the background variables of interest here, as discussed in the next section.

As an example, consider that we are interested in finding the structure of dynamical fields associated with the $22\,\mathrm{m\cdot s^{-1}}$ Kelvin wave at $50\,\mathrm{hPa}$. We first create an index for the $22\,\mathrm{m\cdot s^{-1}}$ Kelvin wave at $50\,\mathrm{hPa}$ (I_wl , where the subscript wl refers to a wavelet based index) and then project a selected dynamical field Y (e.g., zonal wind anomaly) on this index. Yet, if we need to find the structure of the wave signal only when the background flow (total wind speed) U has a specific value (e.g., $11\,\mathrm{m\cdot s^{-1}}$, which is half of the specified wave speed), then we create a regression model relating the wavelet-filtered base index with fields of data in a way that allows the slope coefficients to vary continuously with the background flow indexes as follows:

- 1 Regress the time series square of the $22 \,\mathrm{m\cdot s^{-1}}$ Kelvin-wave index on the total wind along the Equator at 50 hPa (to extract the relationship between wave variance and the background flow) $I_{\rm wl} \times I_{\rm wl} = UC_{\rm var}$.
- 2 Regress the time series of the products of the $22\,\mathrm{m\cdot s^{-1}}$ Kelvin-wave index and any dynamical field (zonal wind anomaly, geopotential anomaly, etc.) that we are interested to find its pattern on the same total wind at 50 hPa (hence, we get the relationship between the covariance and the background flow), $I_{\mathrm{vl}} \times Y = UC_{\mathrm{cov}}$.
- 3 Substitute the value of the background wind, $U_i = 11 \,\mathrm{m\cdot s^{-1}}$, in the regression model in step 1 to find the estimated variance in the given background state $(\mathrm{Var}(U_i) = U_i \times C_{\mathrm{var}})$ and also substituting the same background speed in the regression model in step 2 to find the estimated covariance in the same state $(\mathrm{Cov}(U_i) = U_i \times C_{\mathrm{cov}})$,
- 4 Lastly, we get the slope coefficient when the background wind speed is $11\,\mathrm{m\cdot s^{-1}}$ by dividing the estimated covariance by the estimated variance $(\mathrm{Cov}(U_i))/\mathrm{Var}(U_i)$) calculated in step 3. The resulting regression maps show the waves at the base pressure level and longitude base point that occur at that speed and in the given base state. A regressed signal seen at other pressure levels or at distance from the base point shows the part of the remote signal that is correlated in time with the signal near the base point. This remote signal will generally include altered wave number characteristics (which indicate changes in phase speed as the waves move between environments).

Following Paul (2017a), we use a non-parametric bootstrap test. Our objective is to test whether the varying regression coefficient is statistically different from zero, assuming the null hypothesis of no relationship. For this,

10,000 samples of the wavelet index are created with replacement (see Wilks, 2011, chap. 5) and then 10,000 regression coefficients are calculated, which form the sampling distribution against which the null value of zero is compared. We use the 90% confidence level, so if the slope lies between the 500th and 9,500th quantiles then we reject the null hypothesis and the slope is statistically significant at the 90% level. Since these wavelet signals can contain more than just Kelvin waves (e.g., they can also include eastward-advected Rossby waves), conclusions about Kelvin waves are diagnosed not just by statistical significance of a difference from zero but by the extent to which the regressed pattern takes on characteristics consistent with Kelvin waves. For example, a result that shows eastward flow in a trough on the Equator, with cyclonic gyres to the north and south, suggests that Kelvin waves do not dominate wave signals at the given speed in the given background circumstances.

4 | RESULTS

4.1 | Regressed wave structures in different background wind states

Figure 1 shows regressed geopotential and wind anomalies at 50 hPa associated with the $24\,\mathrm{m\cdot s^{-1}}$ filtered wave at the same vertical level, 50 hPa, at specific background wind speeds using the varying regression technique described in Section 3.2. The background wind U is the zonal mean zonal wind at 50 hPa at the Equator. Figure 1 presents the patterns of the $c=24\,\mathrm{m\cdot s^{-1}}$ filtered wave associated with -17, 9, and $17\,\mathrm{m\cdot s^{-1}}$ background flows. The speed adjusted for quasi-Doppler shifting is c-U. Hence, for example, targeting the $30\,\mathrm{m\cdot s^{-1}}$ wave under background wind speed of $30\,\mathrm{m\cdot s^{-1}}$ indicates that the phase speed of the pattern relative to the background flow is zero (which could not be a Kelvin wave, as the intrinsic frequency is zero if there are no dissipation forces).

Figure 1a shows an in-phase relationship between the wind and geopotential, suggesting the presence of a Kelvin wave. The highest amplitudes of the Kelvin wave are over the Indian Ocean, reflecting the location of the base index and the localization of the wave. The in-phase relationship between the geopotential and wind relaxes as the background wind shifts from easterlies (Figure 1a) to westerlies (Figure 1b,c). Also, the meridional wind component intensifies with the strengthening of the background westerly flow. The deviation of the regressed wave from the Kelvin-wave structure described by Matsuno (1966) occurs when the quasi-Doppler-shifted speed c - U is reduced from $41 \text{ m} \cdot \text{s}^{-1}$ to $7 \text{ m} \cdot \text{s}^{-1}$. The same behavior was also found when targeting slower waves (e.g., 20, 16, and

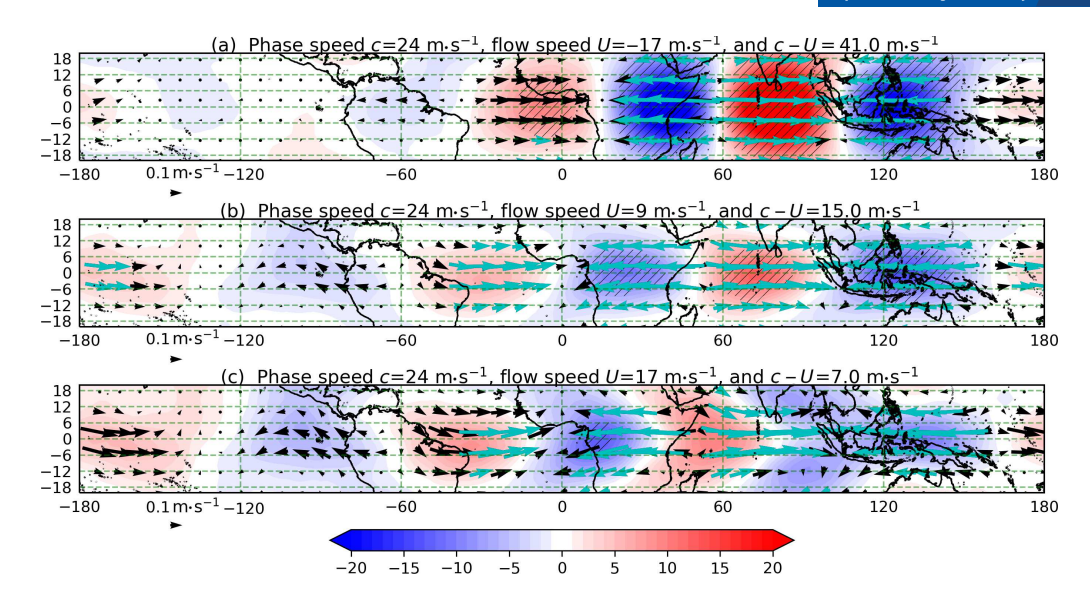


FIGURE 1 Shading represents regressed 50 hPa geopotential with an interval of 1 m²·s⁻² and 50 hPa wind vectors represent wind, with the key wind represents $0.1 \,\mathrm{m\cdot s^{-1}}$. The regressed geopotential and wind are associated with the 24 m·s⁻¹ wave filtered at 50 hPa when the zonal mean zonal wind U at 15 m·s⁻¹ is (a) $-17 \,\mathrm{m\cdot s^{-1}}$, (b) 9 m·s⁻¹, and (c) 17 m·s⁻¹. Red wind vectors and hatched geopotential are statistically significant at the 90% level using the 10,000 samples of the bootstrap test [Colour figure can be viewed at wileyonlinelibrary.com]

14 m·s⁻¹), and the quadrature pattern appears at slower westerly wind background flows as we target slower waves (not shown). The deviation of the in-phase relationship between the zonal wind and geopotential with smaller quasi-Doppler-shifted speeds reflects the fading of the linear Kelvin-wave structure, which encourages us to analyze the wavelet-filtered waves in greater detail at further slower quasi-Doppler-adjusted speeds.

Box-plot diagrams are used to represent the range of the background zonal mean zonal wind at 70, 50, and 30 hPa in Figure 2. The basic state flow at those levels is negatively skewed, consistent with the QBO (Baldwin *et al.*, 2001). As the maximum value of the zonal mean zonal wind at 50 hPa is $17.3 \, \text{m·s}^{-1}$ (see Figure 2), we select wavelet indexes targeting slower phase speeds than the $24 \, \text{m·s}^{-1}$ Kelvin wave shown in Figure 1.

Figure 3 presents regressed geopotential and wind anomalies at 50 hPa associated with the $20\,\mathrm{m\cdot s^{-1}}$ and $16\,\mathrm{m\cdot s^{-1}}$ wave filtered at $50\,\mathrm{hPa}$ when the background speeds are $17\,\mathrm{m\cdot s^{-1}}$ and $15\,\mathrm{m\cdot s^{-1}}$, respectively. The corresponding quasi-Doppler-adjusted phase speeds are $3\,\mathrm{m\cdot s^{-1}}$ and $1\,\mathrm{m\cdot s^{-1}}$, respectively. Negative gepotential anomalies with cyclonic motions straddle the equatorial central and western Indian Ocean, and a latitudinally narrow negative geopotential anomaly with easterlies lies to the east of the equatorial Maritime Continent. This structure is similar to the famous Gill pattern (Gill, 1980). At the aforementioned quasi-Doppler-adjusted speeds, the wavelet index projects on a Gill-like pattern rather the Matsuno Kelvin wave, suggesting the possibility of the absorption of the Kelvin waves that were clearly observed at faster quasi-Doppler-adjusted

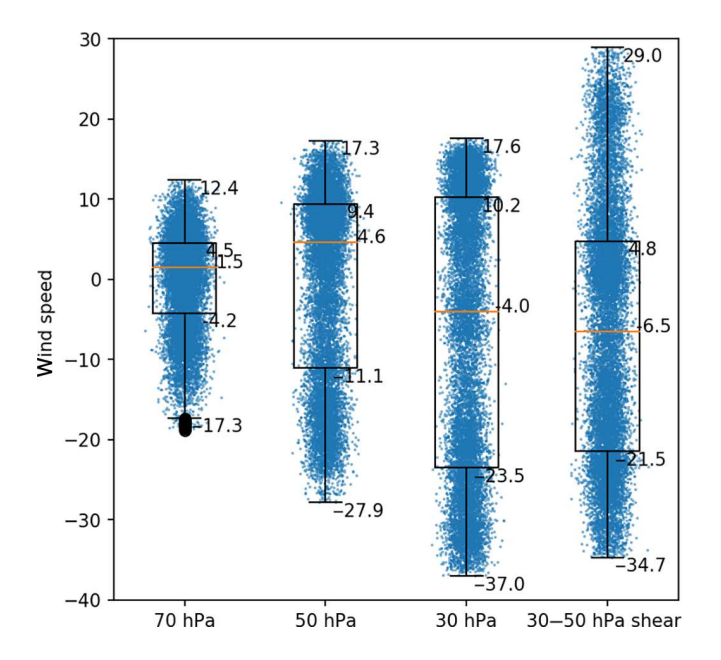


FIGURE 2 Box-plots overlaid with scatter plots of the equatorial zonal mean zonal wind at 70, 50, and 30 hPa and the 30-50 hPa wind shear. The red line inside the box represents the median. The box outlines the first (q1) and third (q3) quartiles, and its width is the interquartile range (IQR). The whiskers' endpoints refer to (q1 – 1.5IQR) and (q3 + 1.5IQR) values, and the points beyond the whiskers are considered outliers. The distribution of the zonal wind is also shown in the scattered dots. The dots are spread randomly in the horizontal within their clusters to make it easier to view the distribution of events along the vertical axis [Colour figure can be viewed at wileyonlinelibrary.com]

394 Quarterly Journal of the SHAABAN AND ROUNDY

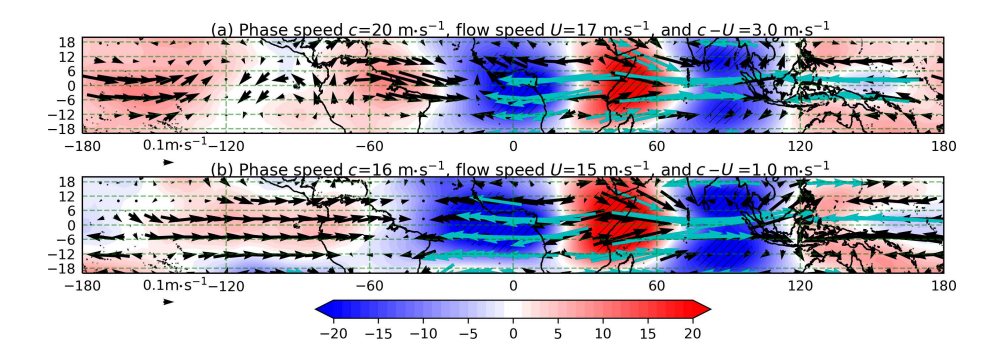


FIGURE 3 As in Figure 1, except (a) the $20 \, \text{m} \cdot \text{s}^{-1}$ Kelvin wave is used when the background speed is $17 \, \text{m} \cdot \text{s}^{-1}$ and (b) the $16 \, \text{m} \cdot \text{s}^{-1}$ is targeted when the background speed is $15 \, \text{m} \cdot \text{s}^{-1}$ [Colour figure can be viewed at wileyonlinelibrary.com]

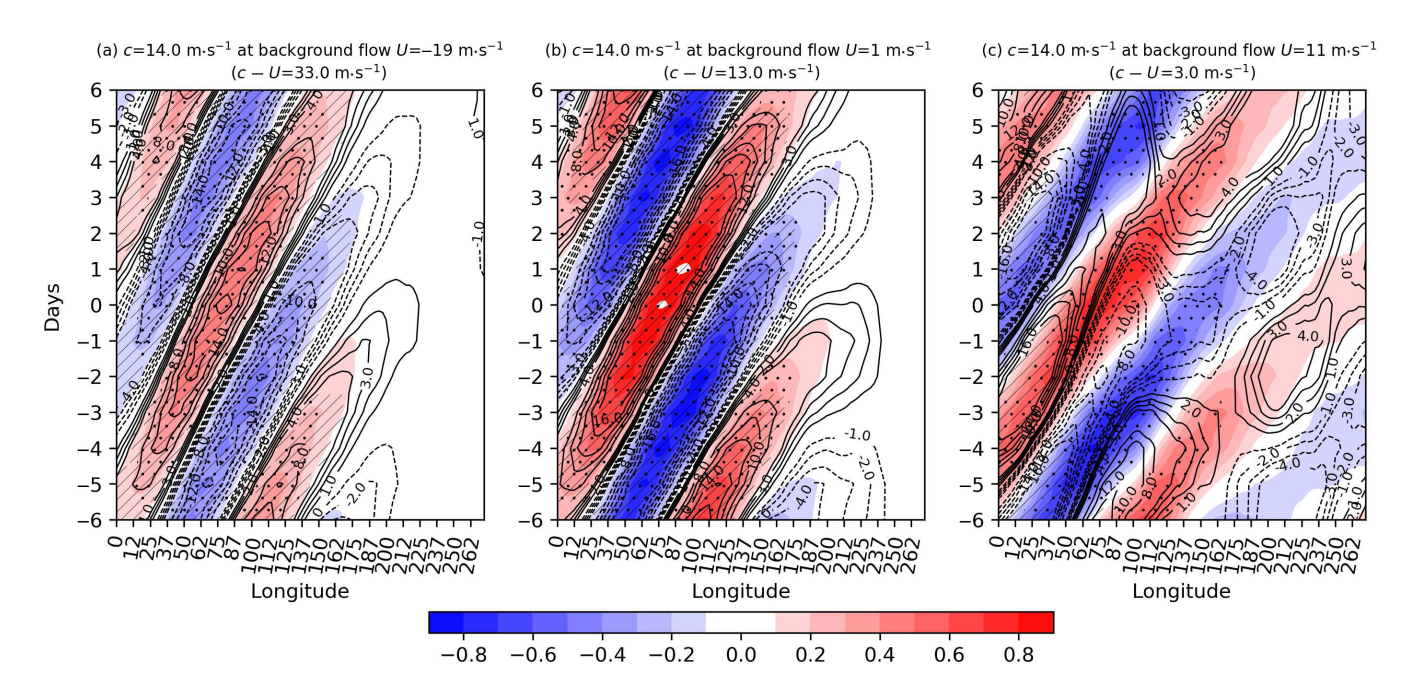


FIGURE 4 Lagged-longitude diagram of regressed zonal wind anomalies (shaded, interval of $0.1~\text{m}\cdot\text{s}^{-1}$) and geopotential anomalies (contours, interval of $1~\text{m}^2\cdot\text{s}^{-2}$ when values between $-4~\text{and}~4~\text{m}^2\cdot\text{s}^{-2}$, and an interval of $2~\text{m}^2\cdot\text{s}^{-2}$ otherwise) averaged between 10° S and 10° N at 50 hPa on the $14~\text{m}\cdot\text{s}^{-1}$ filtered wave at 50 hPa when the background flow at 50 hPa is (a) -19, (b) 1, and (c) $11~\text{m}\cdot\text{s}^{-1}$. Dots and hatching indicate that the zonal wind and geopotential are statistically significant at the 90% level based on a 10,000 sample bootstrap test [Colour figure can be viewed at wileyonlinelibrary.com]

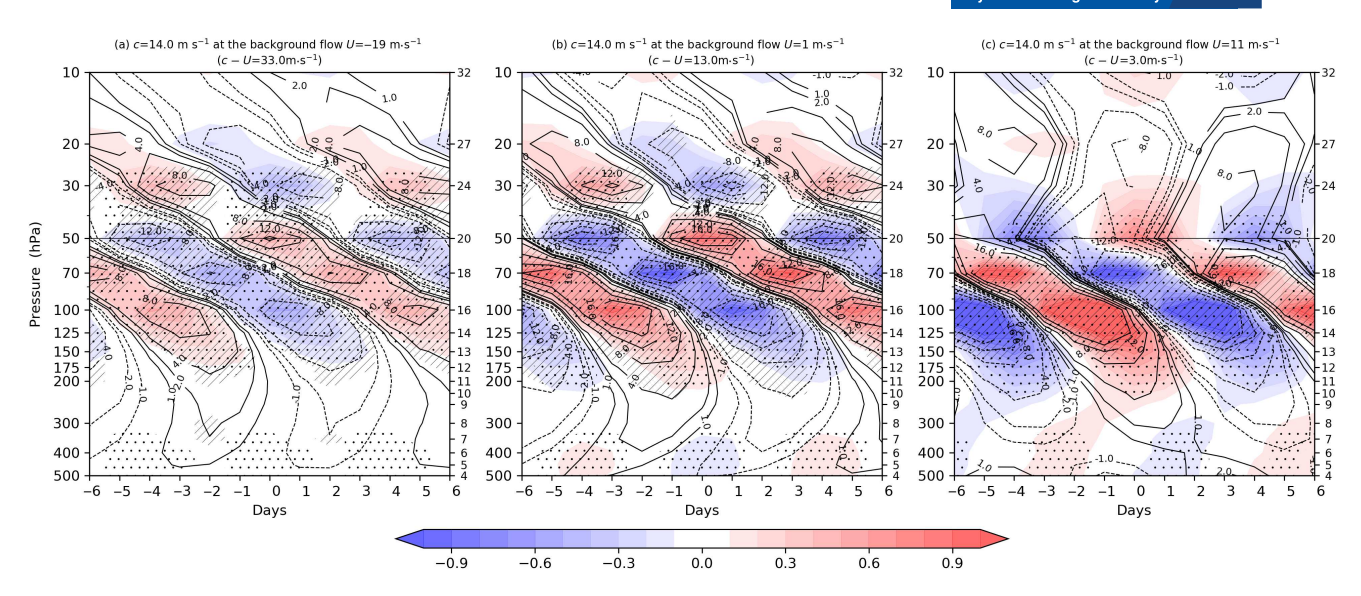
speeds. The Gill-type pattern may be a response of the atmosphere to direct forcing from below under background conditions in which the local atmosphere does not permit a Kelvin wave.

The lagged-longitude structure of the zonal wind and geopotential associated with the $14\,\mathrm{m\cdot s^{-1}}$ Kelvin wave filtered at 50 hPa at different background speeds U is depicted in Figure 4. The phase lines imply an eastward phase velocity. The wave period is ~7 days, consistent with the wavelet frequency, and it does not vary a lot with the background flow. The structure of the Kelvin wave is clear between the $-19\,\mathrm{m\cdot s^{-1}}$ and $+1\,\mathrm{m\cdot s^{-1}}$ background flows, where the quasi-Doppler-shifted speeds are $33\,\mathrm{m\cdot s^{-1}}$ and $13\,\mathrm{m\cdot s^{-1}}$, respectively, as shown in Figure 4a,b. The regressed pattern at $1\,\mathrm{m\cdot s^{-1}}$ background flow depicts a stronger amplitude than the regression against the wavelet base index in $-19\,\mathrm{m\cdot s^{-1}}$ flow. During $11\,\mathrm{m\cdot s^{-1}}$ westerly

flow, the $14\,\mathrm{m\cdot s^{-1}}$ Kelvin wave disappears, as suggested by the quadrature relationship between the zonal wind and the geopotential (which indicates that a Kelvin wave is no longer the dominant signal at that height). This behavior was also observed with the 20 and $16\,\mathrm{m\cdot s^{-1}}$ waves (see Figure 3).

The fading of the Kelvin waves at small quasi-Doppler-shifted speed is a robust dynamical phenomenon, as it was also observed at 30 and 70 hPa using filtered waves at different phase speeds among different background winds. At lower heights, the background wind decreases; thus, slower Kelvin waves could reach the critical layer.

The vertical structure of the regressed waves at different quasi-Doppler-shifted speeds is shown in Figure 5. The lagged-vertical structure of regressed zonal wind and geopotential anomalies is associated with the same wavelet index and background speeds, as in Figure 4.



Lagged-vertical level map of regressed zonal wind anomalies (shaded, interval of $0.1\,\mathrm{m\cdot s^{-1}}$) and geopotential height anomalies (contour, intervals -16, -12, -8, -4, -2, -1, 1, 2, 4, 8, 12, and $16 \text{ m}^2 \cdot \text{s}^{-2}$) on $14 \text{ m} \cdot \text{s}^{-1}$ filtered wave at 50 hPa when the background wind at the same level is (a) -19, (b) 1, and (c) 11 m·s⁻¹. Statistical test is the same as in Figure 4 [Colour figure can be viewed at wileyonlinelibrary.com]

The alternative weakening and strengthening of the zonal wind and geopotential along the phase lines results from the coarse resolution in the vertical and the logarithmic-scale axes in the plotting algorithm. The phase lines imply a downward phase velocity that is consistent with the dynamics of the stratospheric Kelvin wave. Kelvin waves propagate vertically when the quasi-Doppler-shifted speeds are 33 and 13 m·s⁻¹, as presented in Figure 5a,b. Yet, when the background wind is adjusted so that the quasi-Doppler-shifted speed is reduced to 3 m·s⁻¹, a quadrature relationship between zonal wind and geopotential height anomalies suggests that a Kelvin-wave signal is absent, consistent with the hypothesis that it is absorbed below the critical layer.

The structures of regressed waves 4.2 in vertical wind shear with and without critical layer

The association of the vertical shear of the zonal mean zonal wind with the structure of the regressed waves is also analyzed using the same technique used with the varying background winds. The 30-50 hPa vertical shear index is defined as the zonal mean zonal wind at 30 hPa minus that at 50 hPa without dividing by the vertical spacing between the two levels to get more sense of the index values. We replace the background flow index with the 30-50 hPa vertical shear (see Figure 2).

We examine lagged maps of the 14 m·s⁻¹ filtered wave during both westerly and easterly shear at the base, 50 hPa,

and the top (30 hPa) of the 30-50 hPa shear layer. First, we present the 14 m·s⁻¹ wave at 30 hPa during -10 and 18 m⋅s⁻¹ wind shear, as shown in Figure 6a,b. It is clear that the 14 m·s⁻¹ wave maintains the Kelvin-wave structure during the easterly shear (Figure 6a), but it loses this structure during the westerly shear (Figure 6b). The quadrature relationship between the zonal wind and geopotential persists with increasing westerly wind shear (not shown). On the other hand, the structure of the filtered waves at the base of the shear layer (50 hPa; Figure 6c,d) is opposite to that at the top of the shear layer (30 hPa; Figure 6a,b). At the base of the shear layer, Kelvin-wave structure is maintained during the 18 m·s⁻¹ westerly shear (Figure 6c) but disappears at the $-24 \,\mathrm{m\cdot s^{-1}}$ easterly shear (Figure 6d). Yet, Kelvin-wave characteristics are also observed at $-10 \,\mathrm{m \cdot s^{-1}}$ wind shear (not shown). The waves captured at $-24 \,\mathrm{m\cdot s^{-1}}$ (Figure 6d) are slower than the Kelvin wave found during $18 \,\mathrm{m\cdot s^{-1}}$ (Figure 6c). We do not expect that a pattern that deviates from the Kelvin-wave structure would obey the Kelvin-wave dispersion characteristics. To summarize, the Kelvin-wave structure intensifies with the 30-50 hPa westerly shear at 50 hPa and the 30-50 hPa easterly shear at 30 hPa.

The gradual departure of the pattern, at 30 hPa under westerly shear and at 50 hPa with the easterly shear, from the Kelvin-wave structure might be attributed to the gradual reduction of the quasi-Doppler-shifted speed somewhere between 30 and 50 hPa. We found that the 14 m·s⁻¹ wavelet projects on the quadrature pattern under 18 m·s⁻¹ wind shear (see Figure 6). Yet, would the 14 m·s⁻¹ wavelet project on the Kelvin-wave structure if the 18 m·s⁻¹ shear

1477870x, 2023, 751, Downloaded from https://rmets.onlinelibrary.wiley.com/doi/10.1002/qj.4412 by Suny University At Albany, Wiley Online

on Wiley Online Library for rules of use; OA articles are governed by the applicable Creative Commons

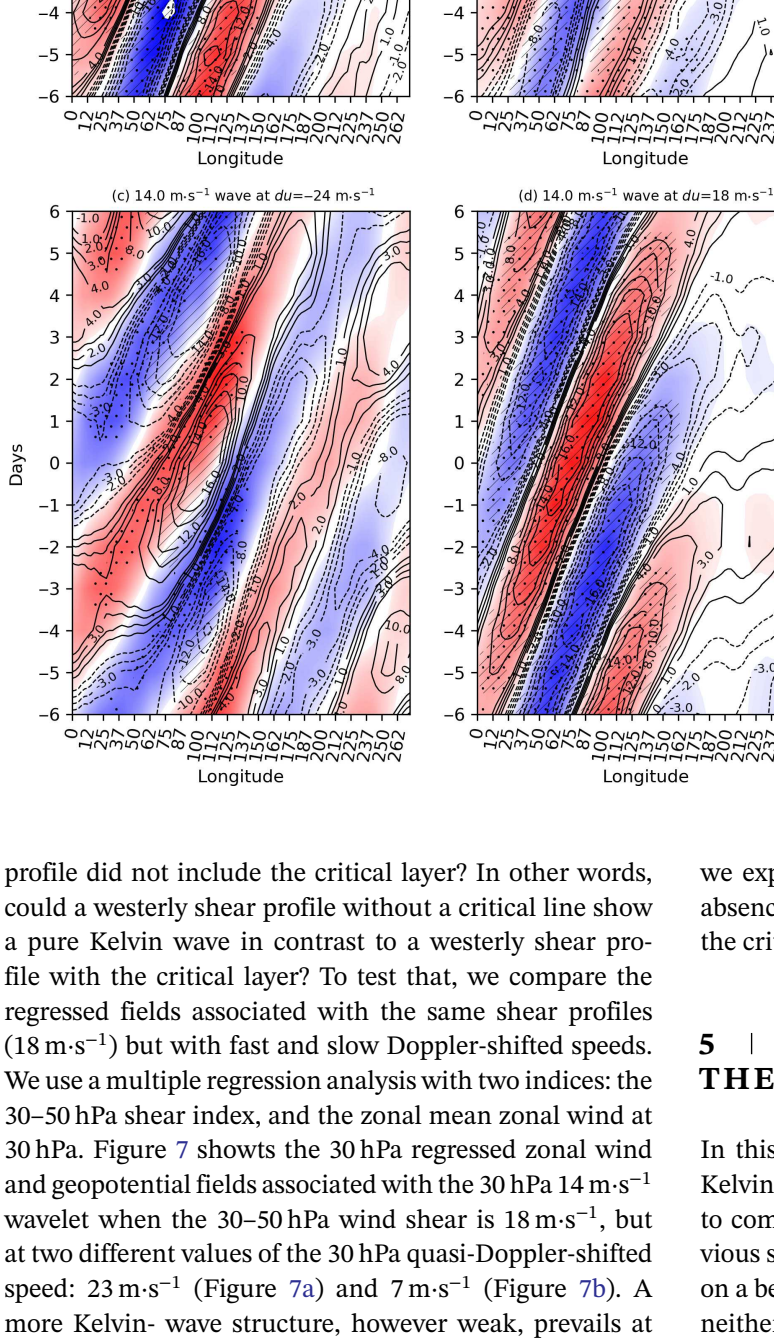


FIGURE 6 Regressed wind (shaded, interval of 0.1 m·s⁻¹) and geopotential (contours, an interval of $1 \text{ m}^2 \cdot \text{s}^{-2}$ when values between -4and $+4 \text{ m}^2 \cdot \text{s}^{-2}$, and an interval of $2 \text{ m}^2 \cdot \text{s}^{-2}$ otherwise) at (a, b) 30 hPa on the 14 m·s⁻¹ Kelvin wave filtered at 30 hPa for (a) $-10 \text{ m} \cdot \text{s}^{-1}$ wind shear and (b) 18 m·s⁻¹ wind shear based on the 30-50 hPa and at (c, d) 50 hPa on the $14 \, \text{m} \cdot \text{s}^{-1}$ Kelvin wave filtered at $50 \text{ hPa for (c)} -24 \text{ m} \cdot \text{s}^{-1} \text{ wind shear}$ and (d) 18 m·s⁻¹ wind shear based on the 30-50 hPa. Dots and hatching have the same meaning as in Figure 4 [Colour figure can be viewed at wileyonlinelibrary.com]

0.60

0.45

0.30

0.15

0.00

-0.15

-0.30

-0.45

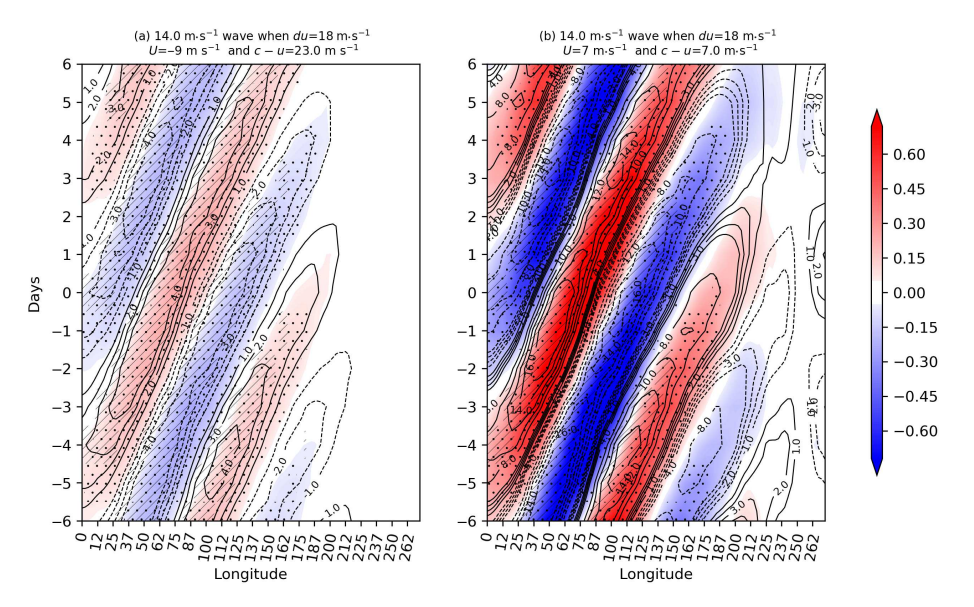
-0.60

0.60 0.45 0.30 0.15 0.00 -0.15-0.30 -0.45-0.60

23 m·s⁻¹ when compared with a semi-quadrature structure that exists at 7 m·s⁻¹. This is somehow different from what we expected, to see a pure Kelvin-wave structure in the absence of the critical line and non-Kelvin structure near the critical layer.

DISPERSION EQUATION OF THE KELVIN WAVE UNDER SHEAR

In this section we derive the dispersion equation of the Kelvin waves under vertical wind shear of the zonal wind to compare the observed wave characteristics in the previous section with the theoretical ones. A primitive model on a beta plane linearized about the zonal mean flow with neither forcing nor dissipation is used following (Andrews et al., 1987, chap. 3, 4). The beta plane approximation is widely used for studying the equatorially confined waves



(Matsuno, 1966; Gill, 1980). The model is as follows:

$$u'_t + \overline{u}u'_x + \overline{u}_z w' + \phi'_x = 0, \tag{2a}$$

$$\beta y u' + \phi_y' = 0, \tag{2b}$$

$$\phi_z' = H^{-1}R\theta' e^{-\kappa z/H}, \qquad (2c)$$

$$u_x' + \rho_0^{-1}(\rho_0 w')_z = 0,$$
 (2d)

$$\theta_t' + \overline{u}\theta_x' + \overline{\theta}_z w' = 0. \tag{2e}$$

The variables u', w', ϕ , and θ' are the zonal wind, vertical wind, geopotential, and potential temperature deviations from the zonal means. The prime and overbar refer to the deviation of the zonal mean and the zonal mean. β is the beta parameter, or the meridional gradient of the Coriolis parameter at the Equator, H is the scale height, and $\kappa \equiv R/c_p$, where R is the gas constant of the dry air and c_p the specific heat at constant pressure. Equations 2a-2c represent the horizontal momentum equations and the hydrostatic equation. Equations 2d and 2e represent the continuity equation and the thermodynamical equation. Note that z is the log-pressure height, which, however close to the geometric height, simplifies the derivations (Andrews et al., 1987; Holton and Hakim, 2012). Following Andrews et al. (1987), we use a solution of the following form to derive the dispersion equations:

$$\begin{pmatrix} u' \\ w' \\ \phi' \\ \theta' \end{pmatrix} = e^{z/2H} \operatorname{Re} \begin{Bmatrix} \hat{u}(y) \\ \hat{w}(y) \\ \hat{\phi}(y) \\ \hat{\theta}(y) \end{Bmatrix} e^{i(kx+mz-\omega t)}, \tag{3}$$

where k and m are the zonal and vertical wave numbers and ω is the angular frequency. We present the dispersion equations in four scenarios in the following subsection.

5.1 | No background wind $\overline{u} = 0$ (and hence no vertical shear $\overline{u}_z = 0$)

Under no background zonal wind $\overline{u} = 0$, the system of Equations 2a-2e reduces to a simple, though very useful and well-known, baroclinic model. From Equations 2e and 2c we get the vertical velocity w' in terms of the geopotential height ϕ' :

$$w' = -\frac{1}{N^2} \phi'_{zt}. \tag{4}$$

From Equation (2a), the geopotential height is related to the zonal wind as $\phi' = (\omega/k)u'$, and another relationship between the zonal wind and geopotential height could be found by substituting w' from the Equation (4) into the continuity equation, Equation (2d). Before proceeding further, we note that (1) the density is a function in the height ($\rho_0 = \rho_s e^{-z/2H}$), where ρ_s is the density at the surface, and (2) we utilize Boussinesq approximation, where i/2H is neglected when compared with the vertical wave number. The Boussinesq approximation is valid for phenomena whose vertical scale (which in this context is the reciprocal of the vertical wave number, m⁻¹) is smaller than the scale height - which is 2H here, as used in the suggested wave solution equation, Equation (3) - of the atmosphere; hence, waves do not feel abrupt reduction of density. For an atmosphere with scale height of roughly 7 km, $1/(2H) \sim 0.07$ km⁻¹, and the vertical wave numbers

are $1.25 \, \text{km}^{-1}$, $0.63 \, \text{km}^{-1}$, $0.31 \, \text{km}^{-1}$, and $0.21 \, \text{km}^{-1}$ for waves of vertical wavelengths 5 km, 10 km, 20 km, and 30 km, respectively. Then, for waves with short vertical wavelengths, |i/2H| < |m|, and the term $[(i/2H) - m] \sim$ -m. The second relationship between the zonal wind and geopotential is

RMetS

$$\phi = \frac{N^2}{m^2} \frac{k}{\omega} u'.$$

From this relationship and Equation (4), we get the Boussinesq dispersion relationship of the Kelvin waves:

$$\frac{\omega}{k} = \pm \frac{N}{m}.\tag{5}$$

For stratospheric (upward energy) Kelvin waves, $\omega/k =$ -N/m, where m < 0. For tropospheric (downward energy) Kelvin waves, $\omega, k = N/m$, where m > 0, under the assumption that the tropopause is not a rigid lid (Ahmed and Roundy, 2021).

Constant background flow with no vertical shear $\overline{u}_z = 0$

The effect of the background flow is recovered when adding the advection terms $\overline{u}u'_{r}$ and $\overline{u}\theta'_{r}$. Hence, the Boussinesq dispersion equation under background zonal wind is

$$\frac{\omega}{k} - \overline{u} = -\frac{N}{m}.\tag{6}$$

The vertical wavelength of the Kelvin waves is directly proportional to the Doppler-shifted phase speed. The calculated vertical wavelengths of the 33 m·s⁻¹, 13 m·s⁻¹, and 3 m·s⁻¹ Doppler-shifted speeds, shown in Figure 5, are \approx 9 km, \approx 3 km, and 785 m, respectively.

Variable background wind 5.3 and vertical wind shear

We complicate the system a little bit by allowing \overline{u} and N to vary with the height and adding back $\overline{u}_z w'$, the only term that incorporates the vertical shear of the zonal wind, to the model. To solve the model, we follow the same steps we did in Section 5.1. We get an equation of the vertical wind in terms of the geopotential height using Equation (2e) (the hydrostatic equation) and Equation (2c) (the thermodynamics equation):

$$w' = \frac{-(\phi'_{zt} + \bar{u}\phi'_{zx})}{N^2}. (7)$$

Then, by substituting the value of w' in the momentum equation of the zonal wind, Equation (2a), and utilizing the Boussinesq approximation, we get

$$\phi' = \frac{\omega - k\overline{u}}{\mathrm{i}\frac{m\overline{u}_z}{N^2}(\omega - k\overline{u}) + k}u'.$$

We also utilize the vertical wind equation (7) in the continuity equation to get another relationship between the gepotential height and the zonal wind.

$$\phi' = \frac{ik}{(im^2N^{-2} - 2N^{-3}N_z m)(\omega - k\overline{u}) - N^{-2}mku_z}u'.$$

From the latter two equations, we solve for $\omega - k\overline{u}$:

$$(c - \overline{u})^2 = \frac{N^2}{m^2 + \frac{2N_z m}{N}}.$$
 (8)

The phase speed changes with height, since the background wind changes with height, yet the vertical wave number does not change with height, though N and N_z may vary with height. This dispersion equation includes an imaginary component in the denominator that could be neglected if we assume that N is constant and hence $N_z = 0$; in this case, this dispersion equation reduces to the classical dispersion equation discussed in the previous section and we consider the background wind as a constant. It is surprising that the dispersion equation of Kelvin waves in settings with a vertical shear of the zonal wind is not a function in the vertical shear of the zonal wind. This might indicate that we need to redesign the wave solution used to solve the model. So, we relax the horizontal and vertical wave numbers so they vary with height, then we derive the dispersion equation again (see next section) and see whether the phase speeds of the Kelvin waves depend on the vertical shear of the zonal wind.

Variable \overline{u} , N, m, and λ 5.4

In this last scenario, we allow the vertical and horizontal wave numbers, besides N and \overline{u} , to vary with the height z. As before, we use Equation (7) to find the relationship between the geopotential height and zonal wind:

$$\phi' = \frac{\omega - \overline{u}k}{AN^{-2}\overline{u}_z(\omega - k\overline{u}) - N^{-2}\overline{u}_z\overline{u}k_z + k}u', \qquad (9)$$

where $A = (1/2H) + i(xk_z + zm_z + m)$. The other relationship between the zonal wind and the geopotential height is

1477870x, 2023, 751, Downloaded

from https://rmets.onlinelibrary.wiley.com/doi/10.1002/qj.4412 by Suny University At Albany, Wiley Online Library on [17.05/2023]. See the Terms and Conditions

-and-conditions) on Wiley Online Library for rules of use; OA articles are governed by the applicable Creative Commons License

found by using Equation (7) and the continuity equation, then:

$$\phi' = \frac{-\mathrm{i}k}{\frac{N^{-2}}{2H} \left[-\mathrm{i}A(\omega - \overline{u}k) + \mathrm{i}\overline{u}k_z \right]} + 2N^{-3}N_z \left[-\mathrm{i}A(\omega - \overline{u}k) + \mathrm{i}\overline{u}k_z \right] - N^{-2} \left[B(\omega - \overline{u}k) - \mathrm{i}A^2(\omega - \overline{u}k) + \mathrm{i}u_z(kA + k_z) + \overline{u}(\mathrm{i}k_{zz} + 2\mathrm{i}k_zA) \right]}$$

$$(10)$$

where $B = xk_{zz} + 2m_z + zm_{zz}$. By equating Equations 9 and 11, we ..." The author original (edited, and modified to give an eqn number) is commented out following this note should they wish to revert to that.

$$\phi' = \frac{-ik}{\frac{N^{-2}}{2H}x + 2N^{-3}N_z x - N^{-2}y}u',$$
(11)

where $x = -iA(\omega - \overline{u}k) + i\overline{u}k_z$ and $y = B(\omega - \overline{u}k)$ $iA^2(\omega - \overline{u}k) + iu_z(kA + k_z) + \overline{u}(ik_{zz} + 2ik_zA),$ $B = xk_{zz} + 2m_z + zm_{zz}$. By equating Equations 9 and 11, we get the following quadratic equation in $\omega - \overline{u}k$:

$$\left(\frac{N^{-2}A}{2H} + 2N^{-3}N_{z}A - N^{-2}iB - N^{-2}A^{2}\right)(\omega - \overline{u}k)^{2} + \left[\frac{-N^{-2}}{2H}\overline{u}k_{z} - 2N^{-3}N_{z}\overline{u}k_{z} + N^{-2}\overline{u}_{z}(KA + k_{z}) + N^{-2}\overline{u}(K_{zz} + 2k_{z}A)\right](\omega - \overline{u}k) + kN^{-2}\overline{u}_{z}\overline{u}k_{z} - k^{2} = 0.$$
(12)

Solving this quadratic dispersion equation is straightforward, though it requires explanation. Hence, we present the following special cases:

1 Constant N, \overline{u} , m, and λ .

As expected, under those conditions, we must get the classical dispersion equation, $c - \overline{u}k = N/m$, discussed in Section 5.2.

2 Constant \overline{u} , m, and λ with varying N.

In this case, the phase speeds of the Kelvin waves reduce to $c - \overline{u} = [N^2/(m^2 + 2imN^{-1}N_z)]^{1/2}$. This dispersion relationship was discussed in Section 5.3. Recall that this dispersion equation was derived in setting with a vertical shear of the zonal wind, though we get this relationship when we assume here that there is no vertical shear. This discrepancy arose cause the terms with the vertical shear of the zonal wind ultimately cancel each other in the derivation.

3 Constant m and λ with varying N and \overline{u} .

$$(c - \overline{u})^2 = -\frac{k\overline{u}_z}{2m}i \pm \frac{kN}{2m}\sqrt{4 - Ri^{-1}}$$
 (13a)

or
$$\omega - k\overline{u} = -\frac{k\overline{u}_z}{2m}i \pm \frac{k\overline{u}_z}{m}\sqrt{Ri - 0.25}$$
, if $\overline{u}_z \neq 0$, (13b)

where $Ri \equiv N^2/\overline{u}_z^2$ is the gradient Richardson number. In the absence of the vertical shear, the dispersion equation under shear, Equation (13a), reduces to ω – $k\overline{u} = -kN/m$. The appearance of the Richardson number is not surprising; it indicates whether the instability caused by the shear is enough to overcome the static stability of the atmosphere. The 0.25 in $\sqrt{\text{Ri} - 0.25}$ is the theoretical threshold distinguishing stable (Ri > 0.25) and unstable flow (Ri < 0.25). The internal gravity wave amplitude was found, by John and Francis (1967), to drop exponentially by $-2\pi\sqrt{\text{Ri}-0.25}$ if the critical level were encountered in a stable flow. The dispersion equation, Equation 13a and 13b, enables us to analyze the variability of the phase speed of the Kelvin waves with the vertical wind shear (as enclosed in Ri). If Ri is less than 0.25, then the Kelvin wave dissipates and $\omega - k\overline{u}$ becomes imaginary, expressing the growth rate of the disturbance

$$\frac{k\overline{u}_z}{2m}\left(-\frac{1}{2}\pm\sqrt{|\mathrm{Ri}-0.25|}\right)$$

which varies proportionally with the wavelength. On the other hand, if Ri is larger than 0.25, then $\sqrt{\text{Ri} - 0.25}$ is real, and the frequency becomes $(k\overline{u}_z/m)\sqrt{\text{Ri}-0.25}$ and the growth rate reduces to $-k\overline{u}_{z}/2m$. The solution of the this model is a combinations of Kummer functions. Figure 8 presents the phase speed of the Kelvin wave as a function in Ri at 4.5 km vertical wavelength. The phase speed of the Kelvin waves increases with the increases of Ri and achieves its maximum speed in the absence of the shear (when Ri reduces to infinity). The Kelvin wave achieves half its maximum speed (its speed in the absence of the shear) when Ri increases from 0.25 to 0.33, and then it approaches 90% of maximum speed when Ri hits 1.32.

The rapid increases of the phase speed of the Kelvin waves with such small increases of Ri motivates us to calculate Ri in the stratosphere. Although the Ri found in the dispersion equation represents the zonal mean, we used data at a specific location, the DYNAMO high-resolution radiosonde observations launched at Addu Atoll airport, Gan island, Maldives, in order to calculate Ri at different fine vertical resolutions,

1477870x, 2023, 751, Downloaded from https://rmets.onlinelibrary.wiley.com/doi/10.1002/qj.4412 by Suny University At Albany, Wiley Online Library on [17/05/2023]. See the Terms and Conditions (https://onlinelibrary.wiley.com/terms

and-conditions) on Wiley Online Library for rules of use; OA articles are governed by the applicable Creative Commons License

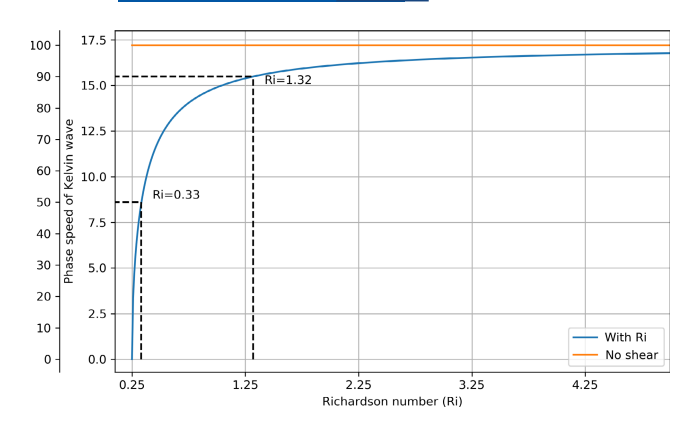


FIGURE 8 Phase speed of the Kelvin wave as a function of the Richardson number. The vertical wavelength of the Kelvin wave is $4.5 \,\mathrm{km}$, and static stability is $0.0240 \,\mathrm{s}^{-1}$. The orange line shows the speed of the Kelvin wave in the absence of vertical wind shear – recall Equation (5). The second y-axis shows the percentage of the phase speed of the Kelvin waves with shear to that without shear [Colour figure can be viewed at wileyonlinelibrary.com]

which is not available at a global scale. Nevertheless, we think that the overall result presented here does not depend on whether we used the zonal-mean or specific-location Richardson number. Figure 9 shows box-plots of unfiltered Ri at the following vertical resolutions: 100, 600, 1,100, 1,600 m. The median, and to a lesser extent, the minimum value of the Ri, increases with the vertical resolution of the data, and it is >1 at all resolutions. The threshold value (0.25) of Ri is found below the lower quartile of Ri when the vertical resolution is 100 and 600 m. Hence, Ri calculated on fine vertical resolution could be associated with a slower Kelvin wave than that associated with a coarse grid. The same conclusion was also observed when analyzing the radiosonde data at different times.

DISCUSSION AND CONCLUSION

The wavelet filtering and the varying-coefficient regression techniques served as tools of precision that enabled us to appoint the targeted wave speed and simultaneously choose the surrounding background wind speed or vertical shear, or both. Three patterns were observed while reducing the quasi-Doppler-shifted speed by targeting different phase-speed-based waves or modifying the background wind. The first observed pattern is the classical Kelvin wave, which appears at high quasi-Doppler-shifted speeds (stronger background easterlies). Then, at slower quasi-Doppler-shifted speeds (weaker background easterlies) we get the second pattern,

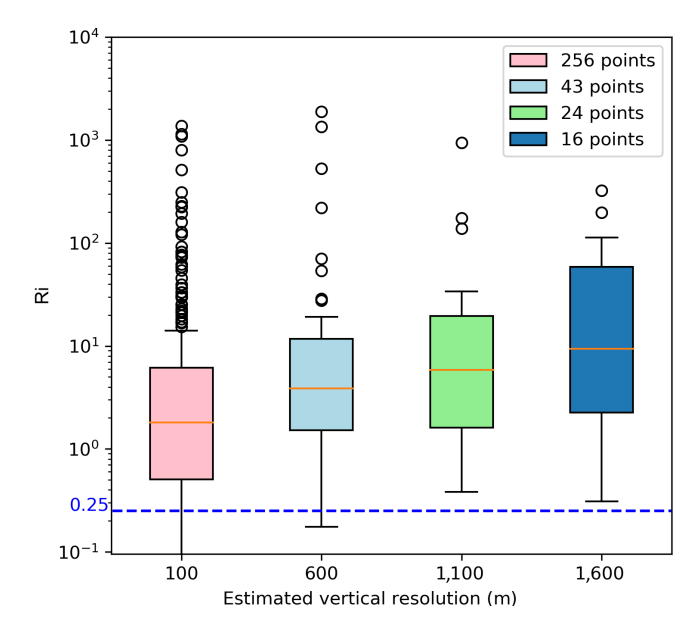


FIGURE 9 Gradient Richardson number calculated using high-resolution radiosonde launched on June 22, 2011, at Addu Atoll airport, Gan Island, Maldives, during the DYNAMO field campaign. The observations are from 199.9 to 5.6 hPa (where the balloon burst). The vertical resolutions are the grid size used to calculate static stability and the vertical shear of the zonal and meridional wind. The circles above the whiskers are the outliers. The red line inside the boxes indicates the median. The legend indicates the number of the points found at the corresponding vertical resolution [Colour figure can be viewed at wileyonlinelibrary.com]

which resembles a quadrature relationship between the wind and the geopotential anomaly. For simplicity, we call the second pattern a "relaxed" Kelvin wave. The "relaxed" Kelvin wave was also found by Paul (2017b) when analyzing the tropospheric Kelvin waves at different phase speeds. This deviation of the slower waves from the traditional tropospheric Kelvin wave expresses the growing role of the convection. Yet, in the stratosphere, the wave dynamics (e.g., intrinsic frequency that is not associated with wave structure similar to Kelvin waves and facing a shear layer) rather than the moist dynamics (e.g., convection-induced convergence that modulates the wave speed and structure) must be responsible for the appearance of the "relaxed" Kelvin wave. Lastly, when the quasi-Doppler-shifted speed reduces to zero or negative values, we get the third pattern, which is the well-known Gill structure (Gill, 1980). The ideal Gill pattern is a forced response, in contrast to the Kelvin wave, which could be a forced response or free (radiated) mode (Harry and Murry, 1994). The transition of the Kelvin wave to the "relaxed" Kelvin structure, and finally to the Gill pattern, reflects the existence of varying frequency sources that could originate from the variation of the background wind in the stratosphere rather than being a direct projection of the tropospheric sources. In other words, a continuum of background speeds might act as a source of intrinsic frequencies. Although the reduction of the quasi-Doppler-shifted speed or wind shear, or both, are, in essence, responsible for the observed patterns, other factors outside the scope of this study might also play a role, like Newtonian cooling or Rayleigh damping, or both.

We found that Kelvin waves fade before approaching the critical layer. Hence, it is intuitive to differentiate between what we suggest as the "observed critical layer" and the "theoretical critical layer." We define the "observed critical layer" as the layer at which the wave structure begins to fade away, and define the "theoretical critical layer" as the layer at which the quasi-Doppler-shifted speed reduces to zero. quasi-Doppler-shifted speed associated with the "observed critical layer" is faster than that associated with the "theoretical critical layer," which is identically zero. This definition, however simple, has a critical implication on our understanding of the eddy-background flow interaction. Actually, waves that are a few meters per second faster than the background flow could be absorbed by the mean flow before approaching the theoretical critical layer. This behavior was also observed by William and Isaac (1991) when studying the absorption of meridional transient tropospheric eddies. The difference between the "theoretical critical layer" and the "observed critical layer" is probably the dissipation factors, like Newtonian cooling and Rayleigh friction that are implicitly taken into account in the "observed critical layer" and which may be associated with the background flow.

We found that Kelvin waves could be absorbed at 30 hPa during 30-50 hPa westerly shear. In general, the absorption of the Kelvin waves is followed by the descent of the westerlies with time, which is a well-known mechanism for the formation of the westerly phase of the QBO (plumb, 1981). We found also that the Kelvin waves could be absorbed at 50 hPa during 30-50 hPa easterly shear. Absorption of the Kelvin waves at the base of the easterly shear layer might be associated with the fluctuation of the tropopause near 100 hPa (Ryu et al., 2008). Although, at the top of the shear layer, Kelvin waves survive during the easterly shear and get absorbed during the westerly shear, multiple linear regression against the background zonal wind and vertical shear did not clearly show whether the existence of the critical line is critical to the absorption of the Kelvin waves. We found that Kelvin waves did not present at the top of the shear layer in westerly shear layer even at fast quasi-Doppler-shifted speed (Figure 7). John (1973) mentioned that internal shear developed inside the wave while propagating in the westerly shear layer and that the fast reduction of the upward group velocity with the increases of the quasi-Doppler speed make it harder

for the Kelvin waves to penetrate further in a westerly shear layer.

The phase speed of the Kelvin waves in a resting atmosphere under the Boussinesq approximation is $c = \pm N/m$. The Boussinesq approximation is expected to be more valid in the troposphere than in the stratosphere, since it is easy find stratospheric Kelvin waves with vertical scales that are way longer than the stratospheric scale height. The reason behind revisiting the dispersion equation is to get more insight into the effect of the vertical wind shear on the phase speed of the Kelvin wave - see Equation 13). Although several studies focused on propagation of the Kelvin waves under vertical and horizontal shear (e.g., Holton, 1970; 1971; Richard, 1972; Alan and Robert, 1982), the variability of the dispersion properties with Richardson number has not gained much attention. In most theoretical studies back in the 1970s and 1980s, Richardson number was assumed to be large, a consequence of the lack of observations with a high vertical resolution in the stratosphere. Under a large Richardson number, we found the dispersion equation under vertical shear reduces to the classical dispersion equation without vertical shear. On the other hand, if the Richardson number lies between 0.25 and 1, the phase speed of the Kelvin wave decreases sharply. Richardson number is more likely to be calculated as small when using observations with fine resolution in the vertical (see Figure 9), which yields estimation biases when using the dispersion equation under vertical shear. The dependence of the calculated bulk Ri on the thickness of the layer used to compute it was hypothesized before - see Reiter and Lester (1967); Elmar and Peter (1968) and references cited therein. The vertical resolution of the data used to calculate Ri depends on the application under investigation. For example, Ri is commonly used in studying clear air turbulence (CAT). (Reiter and Lester, 1967, table 1) lists different studies that correlate the Ri to CAT under different circumstances. The vertical resolutions which vary from study to study; e.g., 250, 300, 1,000 m were chosen to achieve the best correlation between the CAT and Ri. Weisman and Klemp (1982) used a version of the Richardson number to analyze mesoscale convective patterns. The vertical wind shear of the zonal wind was calculated as the difference between the vertical mean zonal wind of the lowest 6km and the vertical mean of zonal wind of the lowest 500 m. This choice was ideal to separate different mesoscale convective patterns. Molinari et al. (2014) used GPS sonde data with a vertical resolution of 400 m to study the outflow of tropical cyclones. We showed that Ri changes with the vertical resolution of the data in the tropical stratosphere (Figure 9), yet the vertical resolution of the reanalysis dataset is still coarse to study the structure of Kelvin waves at various vertical resolutions.

1477870x, 2023, 751, Downbaded from https://mnets.onlinelibrary.wiley.com/doi/10.1002/gj.4412 by Suny University At Albany, Wiley Conline Library on [17.05/2023]. See the Terms and Conditions (https://onlinelibrary.wiley.com/rems-and-conditions) on Wiley Online Library for rules of use; OA article are governed by the applicable Creative Commons Licensea

FUTURE WORK

In a separate study, we will investigate the propagation of Rossby waves under different background flows and vertical shears. Rossby waves are expected to be absorbed when the background wind is easterly instead of westerly.

ACKNOWLEDGEMENTS

This work was funded by the National Science Foundation grant numbers 1560627 and AGS1757342 to Dr Paul Roundy. Comments by Dr George Kiladis improved the presentation of the manuscript. Discussing the dispersion equations of the Kelvin waves with Dr Hing Ong and the Richardson number calculation from high-resolution radiosonde with Dr Michael Gerding was helpful. We are grateful to ECWMF for providing the ERA-Interim dataset, and for NCAR/EOL for providing the DYNAMO high-resolution radiosonde data. We are grateful to the anonymous reviewers, whose comments deepened the discussion in the paper.

CONFLICT OF INTEREST

The authors have no conflict of interest.

ORCID

Ahmed A. Shaaban https://orcid.org/0000-0002-6524-3359

Paul E. Roundy https://orcid.org/0000-0002-2201-0002

REFERENCES

- Andrews, D.G., Leovy, C.B. and Holton, J.R. (1987) Middle Atmosphere Dynamics. International Geophysics, https://books. google.com/books?id=4CPLCQAAQBAJ.
- Baldwin, M.P., Gray, L.J., Dunkerton, T.J., Hamilton, K., Haynes, P.H., Randel, W.J., Holton, J.R., Alexander, M.J., Hirota, I., Horinouchi, T., Jones, D.B.A., Kinnersley, J.S., Marquardt, C., Sato, K. and Takahashi, M. (2001) The quasi-biennial oscillation. Reviews of Geophysics, 39(2), 179-229, https://agupubs. onlinelibrary.wiley.com/doi/abs/10.1029/1999RG000073.
- John, R.B. and Francis, P.B. (1967) The critical layer for internal gravity waves in a shear flow. Journal of Fluid Mechanics, 27(3), 513-539, https://doi.org/10.1017/S0022112067000515.
- Bretherton, F.P. (1966) The propagation of groups of internal gravity waves in a shear flow. Quarterly Journal of the Royal Meteorological Society, 92(394), 466-480, https://rmets.onlinelibrary.wiley. com/doi/abs/10.1002/qj.49709239403.
- Das, U. and Pan, C.J. (2013) Strong Kelvin wave activity observed during the westerly phase of QBO - a case study. Annales Geophysicae, 31(4), 581-590, https://www.ann-geophys.net/31/581/ 2013/.
- Dee, D.P., Uppala, S.M., Simmons, A.J., Berrisford, P., Poli, P., Kobayashi, S., Andrae, U., Balmaseda, M.A., Balsamo, G., Bauer, P., Bechtold, P., Beljaars, A.C.M., van de Berg, L., Bidlot, J., Bormann, N., Delsol, C., Dragani, R., Fuentes, M., Geer, A.J., Haimberger, L., Healy, S.B., Hersbach, H., Hólm, E.V., Isaksen,

- L., Kållberg, P., Köhler, M., Matricardi, M., McNally, A.P., Monge-Sanz, B.M., Morcrette, J.-J., Park, B.-K., Peubey, C., de Rosnay, P., Tavolato, C., Thépaut, J.-N. and Vitart, F. (2011) The era-interim reanalysis: configuration and performance of the data assimilation system. Quarterly Journal of the Royal Meteorological Society, 137(656), 553-597, https://rmets.onlinelibrary.wiley. com/doi/abs/10.1002/qj.828.
- Ern, M. and Preusse, P. (2009a) Wave fluxes of equatorial Kelvin waves and QBO zonal wind forcing derived from saber and ECMWF temperature space-time spectra. Atmospheric Chemistry and Physics, 9(12), 3957-3986, https://www.atmos-chem-phys. net/9/3957/2009/.
- Ern, M. and Preusse, P. (2009b) Quantification of the contribution of equatorial Kelvin waves to the QBO wind reversal in the stratosphere. Geophysical Research Letters, 36(21). https://agupubs. onlinelibrary.wiley.com/doi/abs/10.1029/2009GL040493.
- David, C.F. and Alexander, M.J. (2003) Gravity wave dynamics and effects in the middle atmosphere. Reviews of Geophysics, 41(1). https://agupubs.onlinelibrary.wiley.com/doi/abs/10.1029/ 2001RG000106.
- Gerkema, T., Maas, L.R.M. and van Haren, H. (2013) A note on the role of mean flows in doppler-shifted frequencies. Journal of Physical Oceanography, 43(2), 432-441, https://doi.org/10.1175/ JPO-D-12-0901.
- Gill, A.E. (1980) Some simple solutions for heat-induced tropical circulation. Quarterly Journal of the Royal Meteorological Society, 106(449), 447-462, https://doi.org/10.1002/qj.49710644905.
- Harry, H.H. and Murry, L.S. (1994) The life cycle of the Madden-Julian oscillation. Journal of the Atmospheric Sciences, 51(15), 2225-2237, https://doi.org/10.1175/1520-0469(1994) 051<2225:TLCOTM>2.0.CO;2.
- Holton, J.R. (1970) The influence of mean wind shear on the propagation of Kelvin waves1. Tellus, 22(2), 186-193, https:// onlinelibrary.wiley.com/doi/abs/10.1111/j.2153-3490.1970. tb01520.x.
- James, R.H. and Lindzen, R.S. (1972) An updated theory for the quasi-biennial cycle of the tropical stratosphere. Journal of the Atmospheric Sciences, 29(6), 1076-1080, https://doi.org/10.1175/ 1520-0469(1972)029<1076:AUTFTQ>2.0.CO;2.
- Holton, J.R. and Hakim, G.J. (2012) An Introduction to Dynamic Meteorology, https://books.google.com/books?id= hcxcqQp7XOsC.
- Johnson, R., Schubert, W., Taft, R. and Ciesielski, P. L3 high resolution radiosonde data: Dynamo legacy collection. version 1.0, (2019). https://data.eol.ucar.edu/dataset/347.237.
- Kim, Y.-H. and Chun, H.-Y. (2015a) Momentum forcing of the quasi-biennial oscillation by equatorial waves in recent reanalyses. Atmospheric Chemistry and Physics, 15(12), 6577-6587, https://www.atmos-chem-phys.net/15/6577/2015/.
- Kim, Y.-H. and Chun, H.-Y. (2015b) Contributions of equatorial wave modes and parameterized gravity waves to the tropical QBO in hadgem2. Journal of Geophysical Research: Atmospheres, 120(3), 1065-1090, https://agupubs.onlinelibrary.wiley.com/doi/abs/10. 1002/2014JD022174.
- Richard, S.L. (1970) Internal equatorial planetary-scale waves in shear flow. Journal of the Atmospheric Sciences, 27(3), 394-407, https://doi.org/10.1175/1520-0469(1970)027<0394:IEPSWI> 2.0.CO;2.
- Richard, S.L. (1971) Equatorial planetary waves in shear. Part I. Journal of the Atmospheric Sciences, 28(4:), 609-622,

- https://doi.org/10.1175/1520-0469(1971)028<0609:EPWISP> 2.0.CO:2.
- Richard, S.L. (1972) Equatorial planetary waves in shear:

 Part II. *Journal of the Atmospheric Sciences*, 29(8:),

 1452–1463, https://doi.org/10.1175/1520-0469(1972)029<1452:
 EPWISP>2.0.CO:2.
- Richard, S.L. and James, R.H. (1968) A theory of the quasi-biennial oscillation. *Journal of the Atmospheric Sciences*, 25(6), 1095–1107, https://doi.org/10.1175/1520-0469(1968)025<1095:ATOTQB> 2.0.CO:2.
- Matsuno, T. (1966) Quasi-geostrophic motions in the equatorial area. *Journal of the Meteorological Society of Japan. Ser. II*, 44(1), 25–43, https://doi.org/10.2151/jmsj1965.44.1_25.
- Molinari, J., Duran, P. and Vollaro, D. (2014) Low Richardson number in the tropical cyclone outflow layer. *Journal of the Atmospheric Sciences*, 71(9), 3164–3179, https://journals.ametsoc.org/view/journals/atsc/71/9/jas-d-14-0005.1.xml.
- Narapusetty, B., DelSole, T. and Tippett, M.K. (2009) Optimal estimation of the climatological mean. *Journal of Climate*, 22(18), 4845–4859, https://doi.org/10.1175/2009JCLI2944.1.
- Hamid, A., Pahlavan, Q.F., Wallace, J.M. and Kiladis, G.N. (2021a) Revisiting the quasi-biennial oscillation as seen in era5. Part I: description and momentum budget. *Journal of the Atmospheric Sciences*, 78(3), 673–691, https://journals.ametsoc.org/view/journals/atsc/78/3/JAS-D-20-0248.1.xml.
- Hamid, A.P., John, M.W., Fu, Q. and George, N.K. (2021b) Revisiting the quasi-biennial oscillation as seen in era5. Part II: evaluation of waves and wave forcing. *Journal of the Atmospheric Sciences*, 78(3), 693–707, https://journals.ametsoc.org/view/journals/atsc/78/3/JAS-D-20-0249.1.xml.
- plumb, R.A. (1981) The circulation of the middle atmosphere. *Australian Met Magazine*, 30, 107–121
- Alan R. P. and Robert C. B. (1982) Equatorial waves in steady zonal shear flow. *Quarterly Journal of the Royal Meteorological Society*, 108(456), 313–334, https://rmets.onlinelibrary.wiley.com/doi/abs/10.1002/qj.49710845603.
- William, J.R. and Isaac, M.H. (1991) Phase speed spectra of transient eddy fluxes and critical layer absorption. *Journal of Atmospheric Sciences*, 48(5), 688–697, https://journals.ametsoc.org/view/journals/atsc/48/5/1520-0469_1991_048_0688_pssote_2_0_co_2.xml.
- Elmar, R.R. and Peter, F.L. (1968) Richardson's number in the free atmosphere. *Archiv für Meteorologie, Geophysik und Bioklimatologie, Serie A*, 17(1:), 1–7, https://doi.org/10.1007/BF02250788.
- Reiter, E.R. and Lester, P.F. (1967). The dependence of the Richardson number on scale length, In: *Technical Report 111*: Colorado State University, Atmospheric Science Reports (blue books).
- Paul, E.R. (2017a) Diagnosis of seasonally varying regression slope coefficients and application to the mjo. *Quarterly Journal of the Royal Meteorological Society*, 143(705), 1946–1952, https://rmets.onlinelibrary.wiley.com/doi/abs/10.1002/qj.3054.
- Paul, E.R. (2017b) A wave-number frequency wavelet analysis of convectively coupled equatorial waves and the mjo over the indian ocean. *Quarterly Journal of the Royal Meteorological Society*, https://doi.org/10.1002/qj.3207.

- Paul, E.R. (2020) Interpretation of the spectrum of eastward-moving tropical convective anomalies. *Quarterly Journal of the Royal Meteorological Society*, 146(727), 795–806, https://rmets.onlinelibrary.wiley.com/doi/abs/10.1002/qj.3709.
- Ryu, J.-H., Lee, S. and Son, S.-W. (2008) Vertically propagating Kelvin waves and tropical tropopause variability. *Journal of the Atmospheric Sciences*, 65(6), 1817–1837, https://doi.org/10.1175/2007JAS2466.1.
- Murry, L.S. and Garcia, R.R. (1987) Transient response to localized episodic heating in the tropics. part i: Excitation and short-time near-field behavior. *Journal of the Atmospheric Sciences*, 44(2), 458–498, https://doi.org/10.1175/1520-0469(1987) 044<0458:TRTLEH>2.0.CO;2.
- Ahmed, A.S. and Roundy, P.E. (2021) Upward and downward atmospheric Kelvin waves over the Indian Ocean. *Quarterly Journal of the Royal Meteorological Society*, 147(739), 3154–3179, https://rmets.onlinelibrary.wiley.com/doi/abs/10.1002/qj.4122.
- John, M.W. (1973) General circulation of the tropical lower stratosphere. *Reviews of Geophysics*, 11(2:), 191–222, https://doi.org/10. 1029/RG011i002p00191.
- Weisman, M.L. and Klemp, J.B. (1982) The dependence of numerically simulated convective storms on vertical wind shear and buoyancy. *Monthly Weather Review*, 110(6), 504–520, https://journals.ametsoc.org/view/journals/mwre/110/6/1520-0493_1982_110_0504_tdonsc_2_0_co_2.xml.
- Wheeler, M. and Kiladis, G.N. (1999) Convectively coupled equatorial waves: Analysis of clouds and temperature in the wavenumber–frequency domain. *Journal of the Atmospheric Sciences*, 56(3), 374–399, https://doi.org/10.1175/1520-0469(1999)056<0374:CCEWAO>2.0.CO;2.
- Wheeler, M., Kiladis, G.N. and Webster, P.J. (2000) Large-scale dynamical fields associated with convectively coupled equatorial waves. *Journal of the Atmospheric Sciences*, 57(5), 613–640, https://doi.org/10.1175/1520-0469(2000)057<0613:LSDFAW> 2.0.CO;2.
- Wilks, D.S. (2011) Statistical Methods in the Atmospheric Sciences.
 Academic Press. Elsevier Science, https://books.google.com/books?id=IJuCVtQ0ySIC.
- Yang, G.-Y., Hoskins, B.J. and Slingo, J.M. (2011) Equatorial waves in opposite qbo phases. *Journal of the Atmospheric Sciences*, 68(4), 839–862, https://doi.org/10.1175/2010JAS3514.1.
- Yang, G.-Y., Hoskins, B. and Gray, L. (2012) The influence of the QBO on the propagation of equatorial waves into the stratosphere. *Journal of the Atmospheric Sciences*, 69(10), 2959–2982, https://doi.org/10.1175/JAS-D-11-0342.1.

How to cite this article: Shaaban, A.A. & Roundy, P.E. (2023) On the interaction between Kelvin waves at different phase speeds and the background flow. *Quarterly Journal of the Royal Meteorological Society*, 149(751), 389–403. Available from: https://doi.org/10.1002/qj.4412